

Fig. 1 | Schema of development, testing and validation of the FSA biomarker. To establish a clinically useful resting-state (rs) fMRI biomarker, we addressed several major challenges: (1) obtaining reliable individualized measurements; (2) achieving reproducibility and generalizability across independent populations and sites; (3) achieving biological interpretability and mechanistic plausibility. **a**, The striatal features: based on our hypothesis, three distinct in vivo striatal imaging markers were included to systematically characterize striatal function. **b**, Group-level statistics: statistical analysis was performed for data acquired across multiple MR scanners and demonstrated reproducible FSA patterns. **c**, Individualized prediction of diagnosis: a machine learning model found generalizable predictive patterns of FSA and used them to predict unobserved diagnostic status in independent populations. Using the same classification models, FSA scores were mapped for each patient based on the confidence of the classification as a patient by the models. **d**, Individualized prediction of prognosis: the individualized FSA score predicted the diversity of short-term antipsychotic response in independent populations. **e**, Neurobiological and genetic insights: spatial patterns of elevated striatal spontaneous brain activity were investigated using complementary analyses of molecular imaging and transcriptomic data, revealing a significant spatial association between striatal dopaminergic function and the expression profiles of schizophrenia risk genes. GWAS, genome-wide association study.

from normal to dysfunctional. We hypothesized that FSA would reveal a reliable pathological trait characterizing schizophrenia and would associate with inter-individual variation in antipsychotic response. To test these hypotheses, we applied machine learning and resting-state functional magnetic resonance imaging (fMRI) modalities to infer personalized FSA scores based on connectional and regional functional profiles of the striatum (Fig. 1a). We mapped FSA scores for seven independent cohorts comprising a total of 560 individuals with schizophrenia and 540 matched controls, and validated the FSA measurements by using inter-site cross-validation. Because schizophrenia is associated with presynaptic striatal dopaminergic dysregulation² and evidence suggests that polygenic risk for schizophrenia modulates striatal function^{13,14}, we then integrated multiple modalities to unravel the possible genetic basis of FSA in schizophrenia.

In this work, we propose our new FSA biomarker and show that (1) FSA could reliably distinguish individuals with schizophrenia from healthy controls across different MR scanners (Fig. 1b,c); (2) FSA reliably showed significant heterogeneity within schizophrenia and were moderately sensitive to bipolar disorder, but not to several other neuropsychiatric disorders; (3) FSA robustly predicted the short-term response to antipsychotic medication across different MR scanners (Fig. 1d); (4) abnormal patterns of striatal hyperactivity in schizophrenia were spatially associated with the

striatal dopaminergic system and expression of schizophrenia risk genes (Fig. 1e). The FSA biomarker provides a way forward in prognostic evaluation, clinical stratification and understanding the pathogenesis of schizophrenia.

Results

Group-level identification of FSA. To characterize striatal (dys)function systematically, we used a range of resting-state fMRI markers, including the fractional amplitude of low-frequency fluctuations¹⁵ (fALFF) and regional homogeneity¹⁶ (ReHo), as well as intra- and extra-striatal functional connectivity (FC). These markers provide a multiscale characterization of the striatum, ranging from spontaneous brain activity and internal functional organization to widespread circuit-level connectivity with cortical and subcortical regions. Inference was undertaken to test for between-group differences in each of these markers in adults with schizophrenia, relative to a cohort of age- and sex-matched healthy controls recruited from seven sites (Supplementary Table 1). We found that striatal fALFF and ReHo were significantly increased in the schizophrenia group in each of the seven cohorts (fALFF, Fig. 2a,b; ReHo, Extended Data Fig. 1) and pooled populations (fALFF, $P < 0.0001$; ReHo, $P < 0.0001$) after regressing for age, sex and site (when pooling across sites). The t -statistic for this between-group difference for the striatum was significantly greater than the

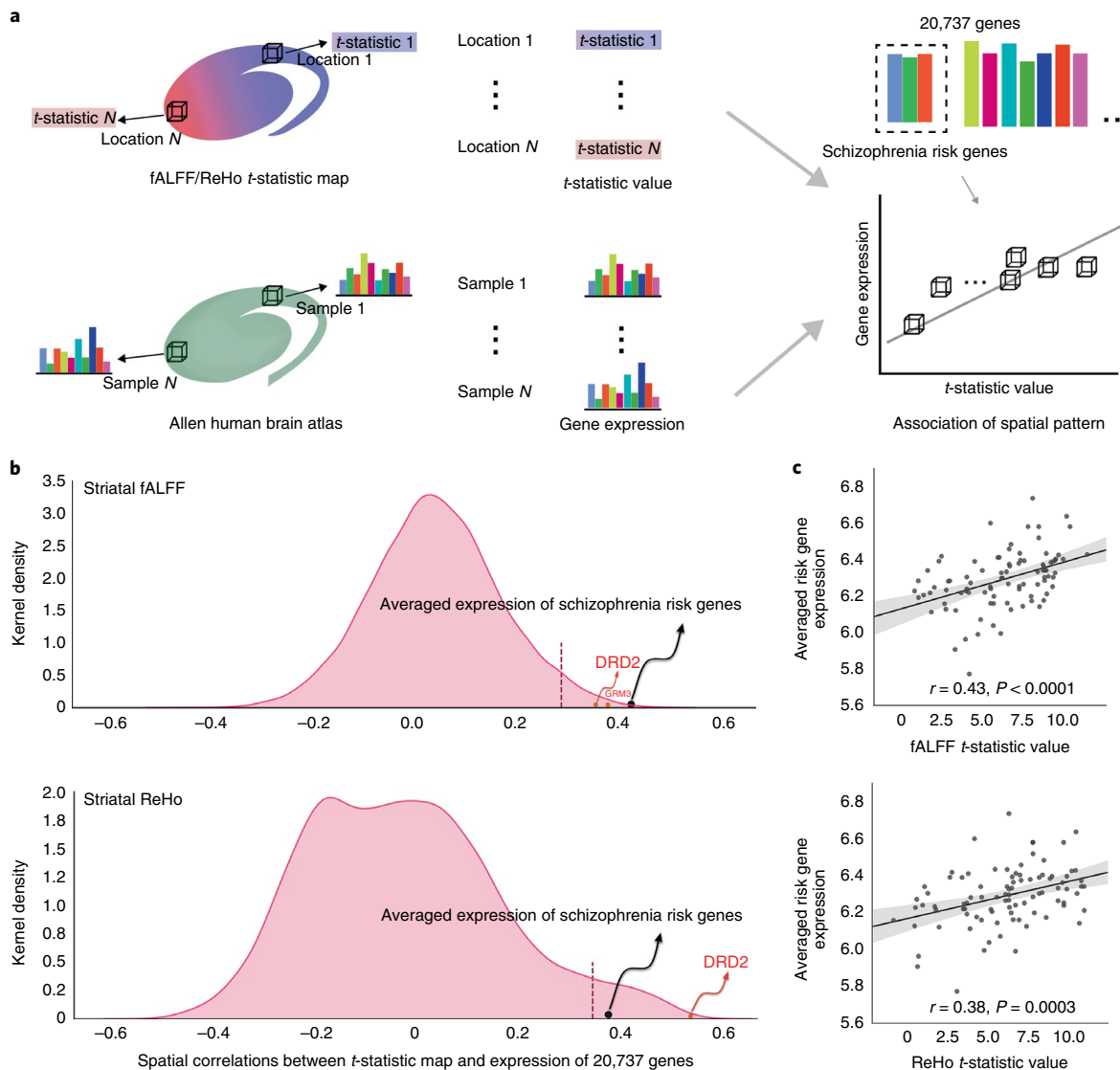


Fig. 4 | Spatial correspondence between gene expression and striatal hyper-activation in schizophrenia. **a**, Schematic of the cross-modal analysis linking gene expression data with striatal imaging data. The t -statistic map indexes voxel-wise differences of fALFF and ReHo between the schizophrenia and healthy control groups (that is, a higher t -statistic value corresponds to a more severe abnormality in this voxel/location). In addition, the Allen Human Brain Atlas provided a spatially defined transcriptional template of the healthy human brain with dense samples in the striatum. We performed this analysis based on the hypothesis that if the fALFF and ReHo t -statistic map showed a significant spatial correlation with the expression pattern of a gene, then the emergence of the striatal hyper-activation in schizophrenia might be related to this gene. **b**, Distribution of spatial correlation (Pearson's correlation) between fALFF (upper) and ReHo (lower) t -statistic maps and regional gene expression profiles sampled within the left striatum ($n=92$), highlighting the significant position of *DRD2* (encoding dopamine receptor D2), *GRM3* (encoding glutamate metabotropic receptor) and averaged schizophrenia risk gene expression. The dashed line separates the top 5% significant genes in the whole gene sets. For fALFF, the correlation between the t -statistic maps and the averaged risk gene expression scores was greater than for any of the 43 risk genes alone, and the gene expression profiles of *DRD2* and *GRM3* were most strongly correlated (among 43 risk genes) across the striatum with the t -statistic maps (*DRD2* $r=0.36, P=0.00045$; *GRM3* $r=0.38, P=0.00017$; Pearson's correlation). *DRD2* gene expression was the most highly correlated schizophrenia risk gene associated with ReHo ($r=0.54, P<0.0001$), ranking 16th among all 20,737 genes. **c**, Scatter plots showing the significant associations (Pearson's correlation) between the average schizophrenia risk gene expression and fALFF (left) and ReHo (right) t -statistic maps computed across selected regional gene expression samples within the striatum. P values based on permutation tests (replace risk genes with 43 randomly selected genes; 10,000 permutations) are shown.

revealed significant enrichment in genes for the regulation of synapses, calmodulin binding and neuronal and synaptic cellular components (Supplementary Figs. 11–13).

Discussion

It is increasingly recognized that clinical, genetic and neurobiological heterogeneity in psychiatric disorders cannot be adequately parsed using current categorical diagnostic criteria. To make

progress in developing new treatments and understanding the underlying causes, multimodal biomarkers are needed that transcend and cut across classic diagnostic categories. This would enable objective measurement of clinical traits that reside on a continuum, from normal to extreme. Here, we have developed a new dimensional biomarker that satisfies these key criteria. To our knowledge, this is the first study to establish and evaluate a neuroimaging biomarker that enables independent cross-scanner characterization of

27. Howes, O. D. et al. The nature of dopamine dysfunction in schizophrenia and what this means for treatment. *Arch. Gen. Psychiatry* **69**, 776–786 (2012).
28. Chen, K. C. et al. Striatal dopamine transporter availability in drug-naïve patients with schizophrenia: a case-control SPECT study with [^{99m}Tc]-TRODAT-1 and a meta-analysis. *Schizophr. Bull.* **39**, 378–386 (2013).
29. Schizophrenia Working Group of the Psychiatric Genomics Consortium. Biological insights from 108 schizophrenia-associated genetic loci. *Nature* **511**, 421–427 (2014).
30. Garcia-Gomez, F. J. et al. Elaboration of the SPM template for the standardization of SPECT images with ¹²³I-ioflupane. *Rev. Esp. Med. Nucl. Imagen Mol.* **32**, 350–356 (2013).
31. Grecchi, E., Doyle, O. M., Bertoldo, A., Pavese, N. & Turkheimer, F. E. Brain shaving: adaptive detection for brain PET data. *Phys. Med. Biol.* **59**, 2517–2534 (2014).
32. Hawrylycz, M. J. et al. An anatomically comprehensive atlas of the adult human brain transcriptome. *Nature* **489**, 391–399 (2012).
33. Watanabe, K., Taskesen, E., van Bochoven, A. & Posthuma, D. Functional mapping and annotation of genetic associations with FUMA. *Nat. Commun.* **8**, 1826 (2017).
34. Howes, O. D. et al. Treatment-resistant schizophrenia: Treatment Response and Resistance in Psychosis (TRIP) Working Group consensus guidelines on diagnosis and terminology. *Am. J. Psychiatry* **174**, 216–229 (2017).
35. Roberts, D. L. & Velligan, D. I. Medication adherence in schizophrenia. *Drug Discov. Today Ther. Strateg.* **8**, 11–15 (2011).
36. Zhang, J. P. et al. Schizophrenia polygenic risk score as a predictor of antipsychotic efficacy in first-episode psychosis. *Am. J. Psychiatry* **176**, 21–28 (2019).
37. Frank, J. et al. Identification of increased genetic risk scores for schizophrenia in treatment-resistant patients. *Mol. Psychiatry* **20**, 150–151 (2015).
38. Kaar, S. J., Natesan, S., McCutcheon, R. & Howes, O. D. Antipsychotics: mechanisms underlying clinical response and side-effects and novel treatment approaches based on pathophysiology. *Neuropharmacology*, 107704 (2019); <https://doi.org/10.1016/j.neuropharm.2019.107704>
39. Valenti, O., Cifelli, P., Gill, K. M. & Grace, A. A. Antipsychotic drugs rapidly induce dopamine neuron depolarization block in a developmental rat model of schizophrenia. *J. Neurosci.* **31**, 12330–12338 (2011).
40. Jauhar, S. et al. The effects of antipsychotic treatment on presynaptic dopamine synthesis capacity in first-episode psychosis: a positron emission tomography study. *Biol. Psychiatry* **85**, 79–87 (2019).

Publisher's note Springer Nature remains neutral with regard to jurisdictional claims in published maps and institutional affiliations.

© The Author(s), under exclusive licence to Springer Nature America, Inc. 2020

figures and wrote the manuscript. A.Z. and O.H. made substantial contributions to the manuscript and provided critical comments. A.Z., W.Y., X.W., O.H., H.Y., Y.L., L.F., K.J.W., J.L., S.L., M.W., Y. Sun, M.S. and T.J. participated in discussions of the results and the manuscript. G.R. developed the website. P.L., J.C., Y.C., W.Y., H.Y., H.N.W., W.L., Z.L., Y.Y., H.G., P.W., L. Lv, L. Lu, J.Y., Y. Song, H.L.W., H.Z., H.W., Y.N., Y.D., Y.C., J.X., X.X. and D.Z. contributed to the data acquisition.

Competing interests

The authors declare no competing interests.

Additional information

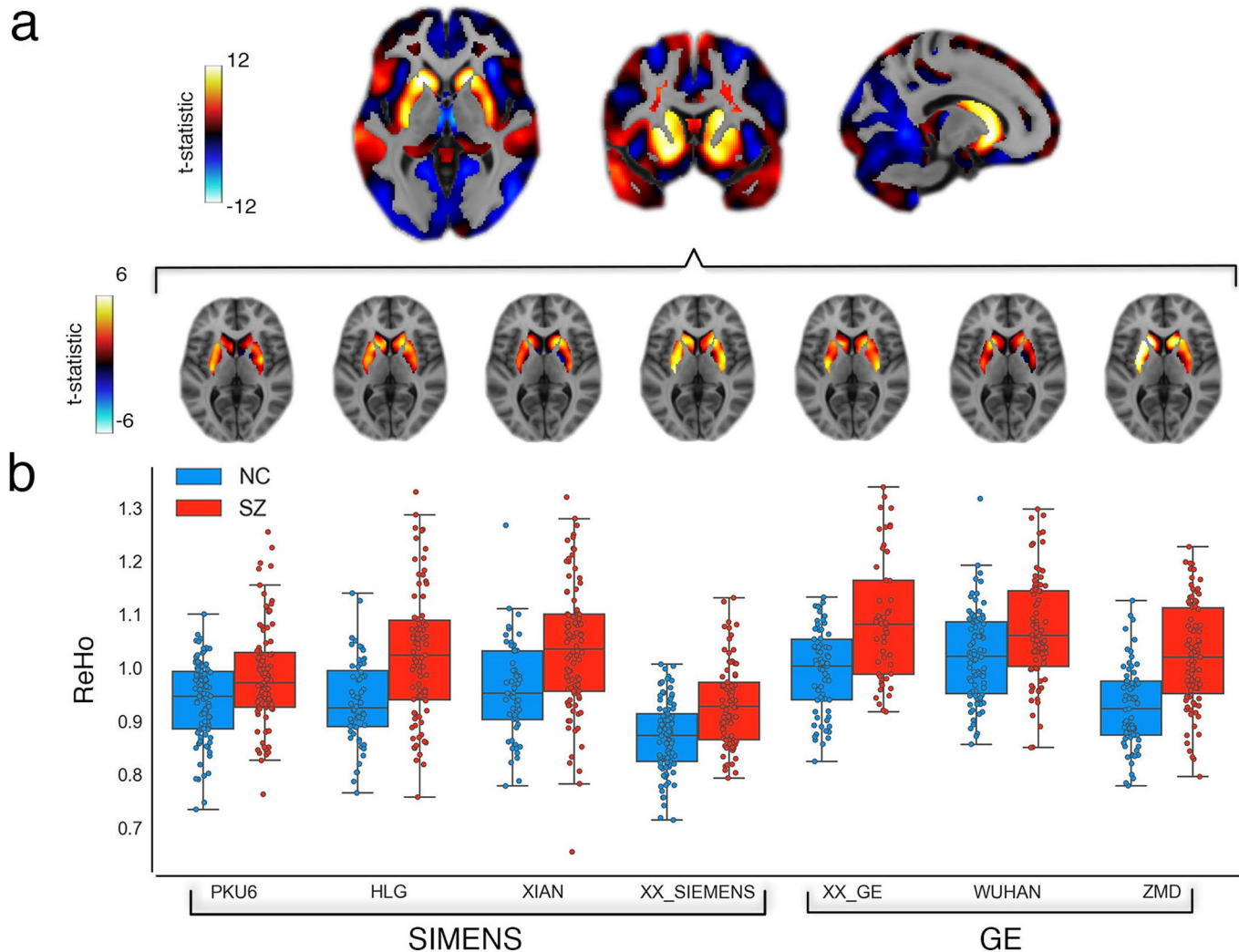
Extended data is available for this paper at <https://doi.org/10.1038/s41591-020-0793-8>.

Supplementary information is available for this paper at <https://doi.org/10.1038/s41591-020-0793-8>.

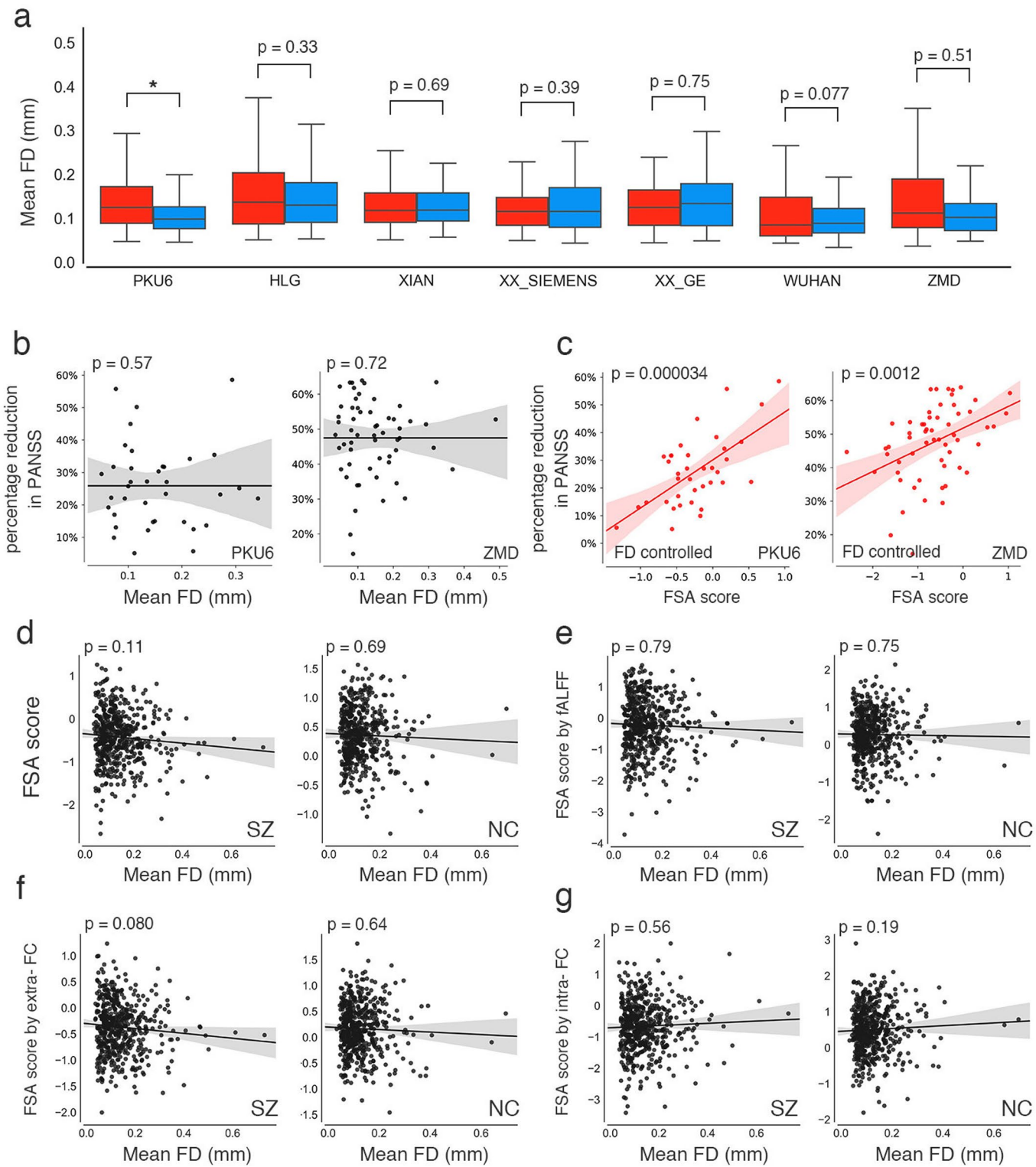
Correspondence and requests for materials should be addressed to T.J. or B.L.

Peer review information Kate Gao was the primary editor on this article, and managed its editorial process and peer review in collaboration with the rest of the editorial team.

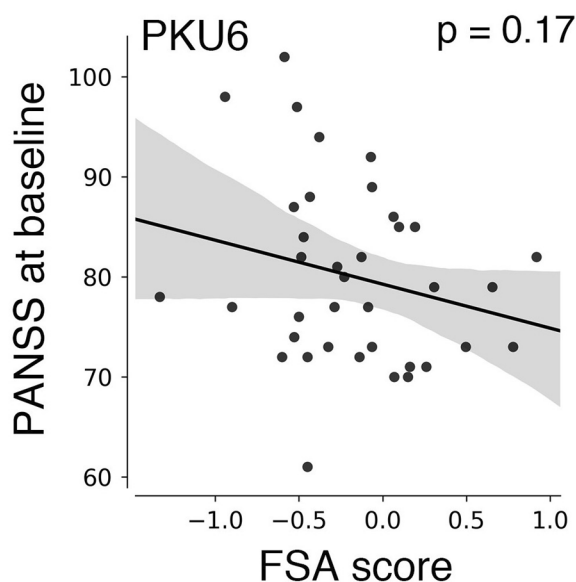
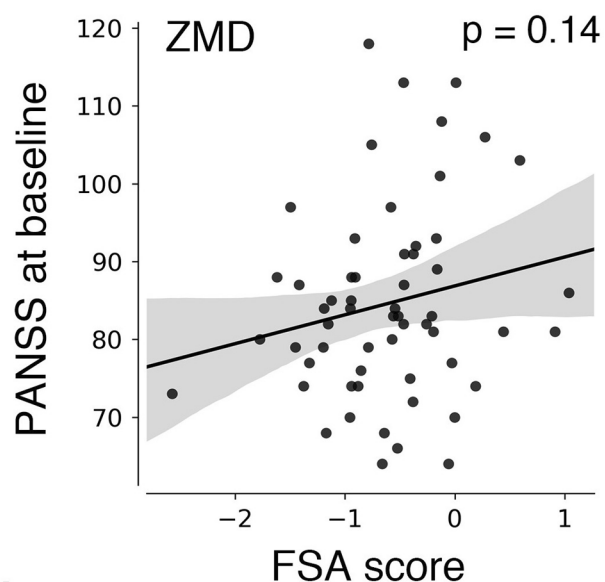
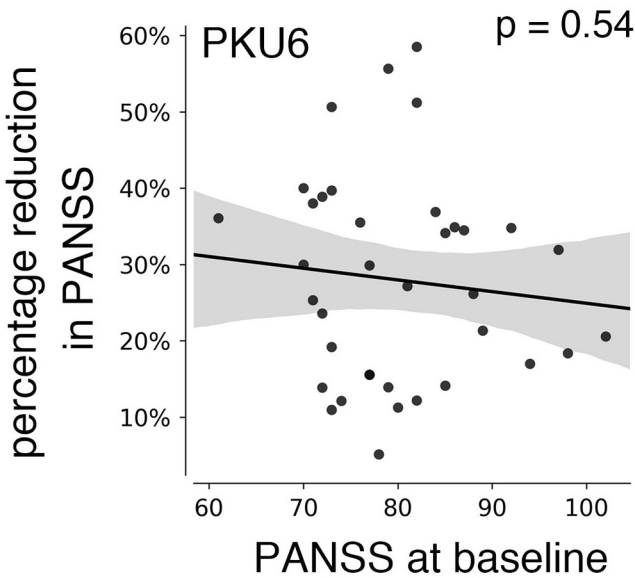
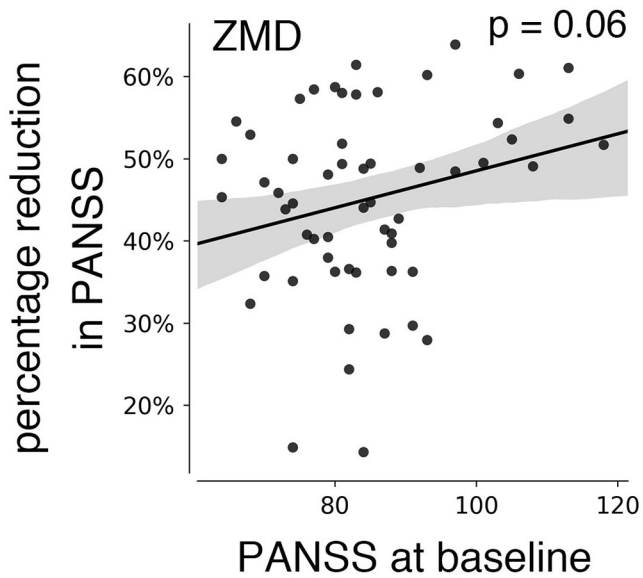
Reprints and permissions information is available at www.nature.com/reprints.



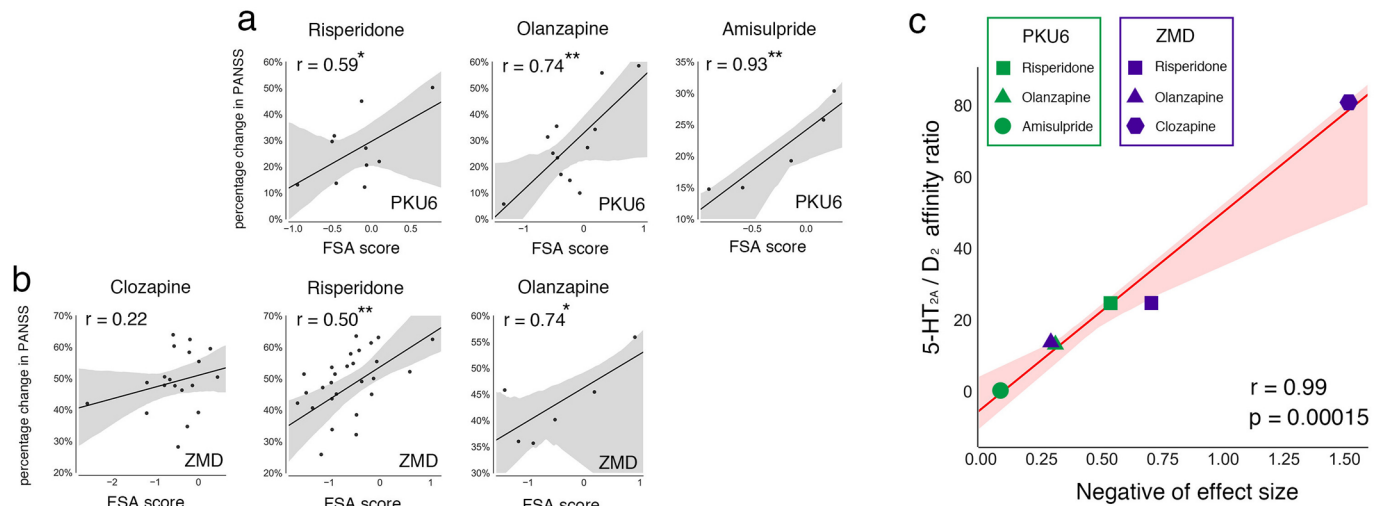
Extended Data Fig. 1 | Elevated regional homogeneity (ReHo) in schizophrenia. **a**, Map of t-statistic values for between-group difference in ReHo (schizophrenia group minus healthy comparison group; unpaired two-sided t-test). n = 560 subjects with schizophrenia and n = 540 controls. **Top:** Data pooled across all seven scanners. The largest t-statistic values were for areas within the striatum, indicating that the striatum is a focal point of significantly increased ReHo in schizophrenia. **Bottom:** Data analyzed independently for each of the seven scanners. Only t-statistic values within the striatum are shown. Each axial slice ($z=5$) corresponds to data acquired from an independent scanner. Images ordered according to Panel b. **b**, Scatter-box chart of the mean fALFF in the striatum of normal controls (NC, shown in blue) and schizophrenia groups (SZ, shown in red) across different scanners. From left: Peking University Sixth Hospital (SIMENS scanner, $P < .0003$; n = 92 SZ, n = 98 NC), Beijing Huilongguan Hospital (SIMENS scanner, $P < 5 \times 10^{-6}$; n = 83 SZ, n = 59 NC), Xijing Hospital (SIMENS scanner, $P < 1 \times 10^{-4}$; n = 90 SZ, n = 54 NC), Henan Mental Hospital (SIMENS scanner, $P < 4 \times 10^{-8}$; n = 81 SZ, n = 102 NC), Henan Mental Hospital (GE scanner, $P < 6 \times 10^{-7}$; n = 49 SZ, n = 69 NC), Renmin Hospital of Wuhan University (GE scanner, $P = .00025$; n = 82 SZ, n = 89 NC), and Zhumadian Psychiatric Hospital (GE scanner, $P < 7 \times 10^{-10}$; n = 83 SZ, n = 69 NC). Striatal hyperactivity indicated by increased ReHo in the schizophrenia group is evident in samples from all sites despite having been acquired using different scanners. Significance was assessed by unpaired two-sided t-test and there was no adjustment for multiple testing. The sample size and definition of boxplot are consistent with those in Fig. 2b.



Extended Data Fig. 2 | Impacts of intra-scan head motion confound on FSA. **a**, Boxplot of mean framewise distance (FD) for schizophrenia (red) and healthy comparison (blue) groups. As indicated by the asterisk, the mean FD of FSA was significantly higher in the schizophrenia group in PKU6 hospital ($P < .05$, unpaired two-sided t-test). No significant difference in FD between schizophrenia group and healthy controls in other cohorts (P values are shown in the figure; unpaired two-sided t-test). The sample size and definition of boxplot are consistent with those in Fig. 2b. **b**, Scatter plots showing the absence of a significant correlation between percentage change in PANSS symptom severity and mean FD (PKU6 hospital: $P = .57$, $n = 37$; ZMD hospital: $P = .72$, $n = 58$). **c**, Scatter plots showing the partial correlation between percentage change in PANSS symptom severity and the FSA score, controlling for the effect of mean FD (PKU6 hospital: $P = .000034$, $n = 37$; ZMD hospital: $P = .0012$, $n = 58$). **d**, Relationship between the FSA score and mean FD. **e-g**, Relationship between mean FD and the FSA score based on fALFF, intra-striatal FC and extra-striatal FC. Pearson correlation were used to assess significance in Panels b-g.

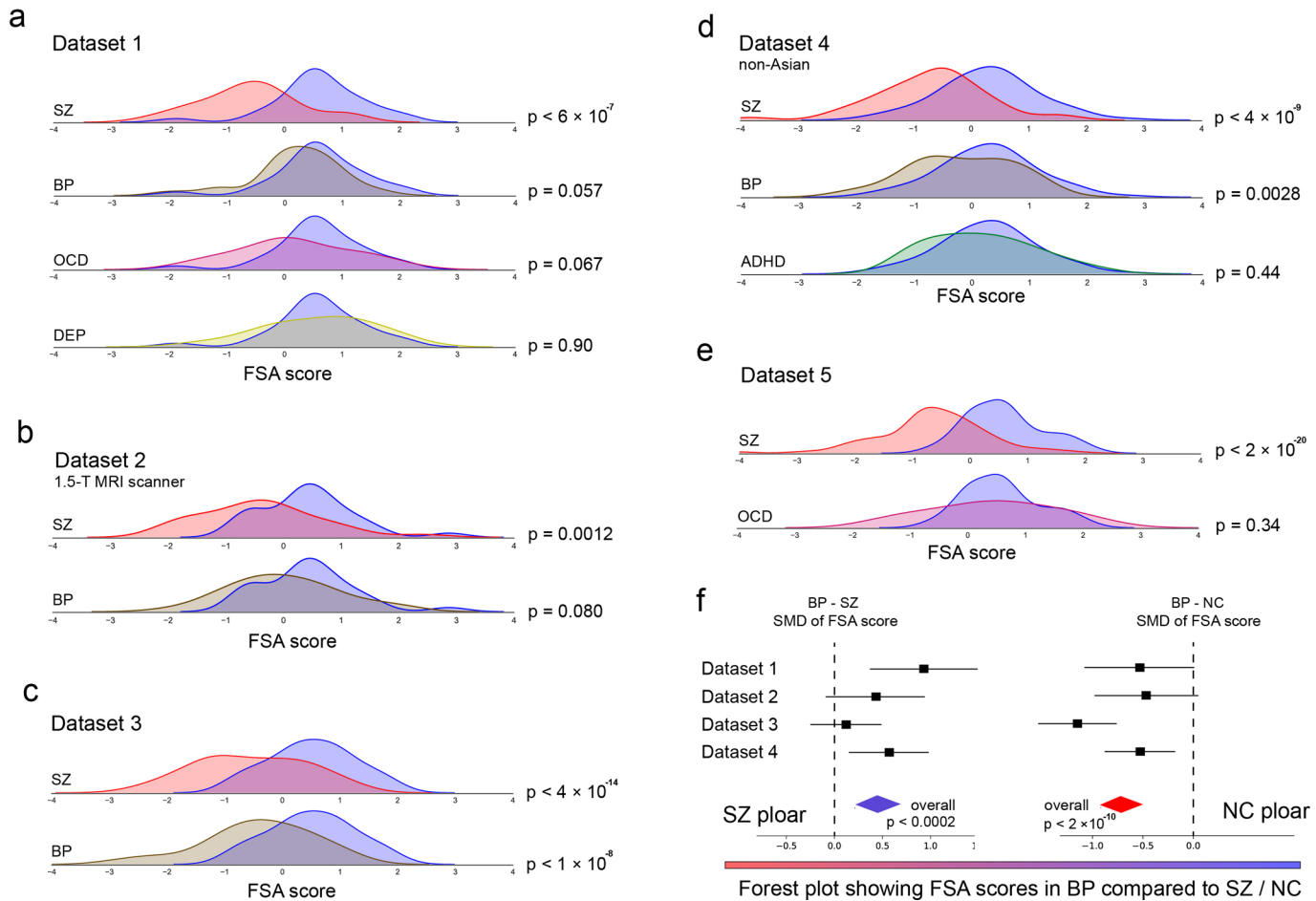
a**b****c****d**

Extended Data Fig. 3 | Impacts of baseline symptom on FSA and percentage symptom reduction. **a, b**, No significant correlation between the FSA score and PANSS at baseline in longitudinal cohorts from either PKU6 hospital or ZMD hospital. **c, d**, No significant correlation between the FSA at baseline and the percentage reduction in PANSS in longitudinal cohorts from either PKU6 hospital or ZMD hospital. For Panels a-d: $P > .05$; Pearson correlation; n=37 in PKU6 hospital and ZMD hospital n=58 in ZMD hospital.

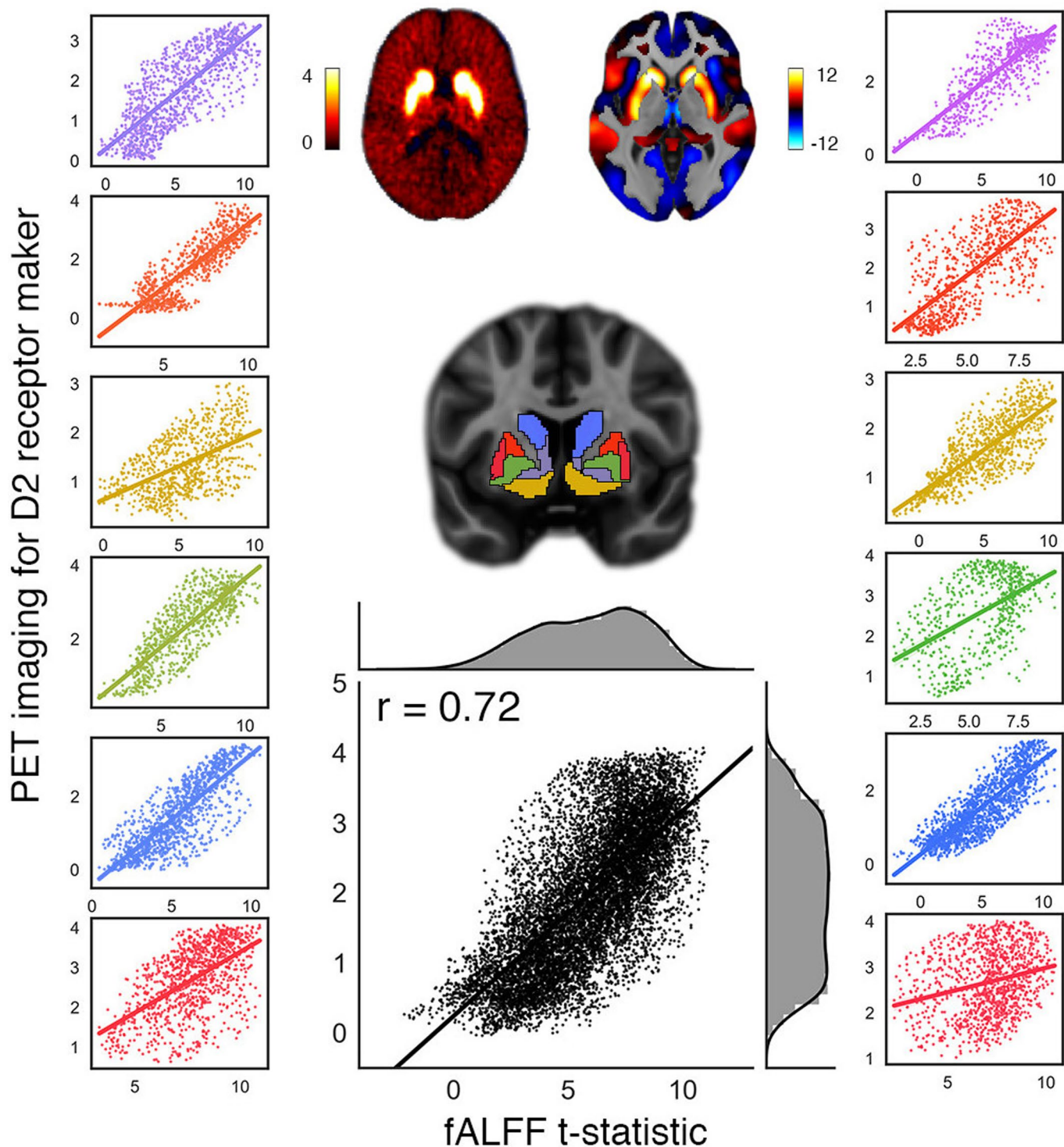


Extended Data Fig. 4 | Prognostic utility of FSA stratified according to antipsychotic categories. The relationship between percentage reduction in PANSS and the FSA score stratified according to antipsychotic category. All the antipsychotic categories with more than (or equal to) 5 patients were analyzed and Pearson's r was represented. **a**, subjects with schizophrenia in PKU6 hospital, $n=10$ Risperidone, $n=12$ Olanzapine, $n=5$ Amisulpride. **b**, subjects with schizophrenia in ZMD hospital, $n=19$ Clozapine, $n=29$ Risperidone, $n=6$ Olanzapine. The single asterisk (*) and double asterisks (**) indicate $P < .1$ and $P < .05$, respectively. **c**, The linear relationship between the 5-HT_{2A} / D₂ affinity ratio and the negative of effect size (the natural logarithm of Pearson's r) of FSA correlated with the antipsychotic response in specific medication group ($n=6$, Pearson correlation).

Assessment of FSA in other diagnostic and ethnic categories



Extended Data Fig. 6 | FSA in previously unused datasets characterized by different MR parameters, ethnicities or disease categories. Density plots show FSA scores computed in five independent datasets (Validation datasets 1-5) comprising individuals with schizophrenia, bipolar disorder, depression, OCD, and ADHD. Groups comprising healthy comparison individuals are shown in blue. To aid visualization, FSA was normalized separately for each dataset. Specifically, we first standardized the FSA scores in individuals with schizophrenia and healthy controls, and then aligned the standardized model for FSA score in other diagnostic groups. Comparisons were made by unpaired two-sided t-test in Panels a-f. **a**, Dataset 1: FSA scores for individuals with schizophrenia ($n=30$), but not bipolar disorders (BP, $n=25$), OCD ($n=30$) or depression (DEP, $n=27$), significantly differed from those of healthy controls ($n=29$). **b**, Dataset 2: FSA generalizes to a 1.5-T MRI scanner. The FSA scores for individuals with schizophrenia ($n=30$) were significantly different from those of healthy controls ($n=29$); Furthermore, individuals with bipolar disorder ($n=30$) showed a trend toward significantly lower FSA scores compared to controls ($P=.080$). **c**, Dataset 3: Both individuals with schizophrenia ($n=81$) and bipolar disorder ($n=41$) showed significantly lower FSA scores compared to healthy controls ($n=102$), and FSA scores did not differ significantly between the schizophrenia and bipolar groups. **d**, Dataset 4: FSA generalizes to non-Han Chinese ethnicities. Both individuals with bipolar disorder ($n=45$) and schizophrenia ($n=47$) showed significantly lower FSA scores compared to healthy controls ($n=115$), whereas individuals with ADHD ($n=39$) did not differ from controls. **e**, Dataset 5: FSA scores for individuals with bipolar disorder compared with individuals with schizophrenia or healthy controls. The sample sizes in Datasets 1-4 were described above. SMD = standardized mean difference. The relative effect sizes were calculated as standardized mean differences (Hedges' g) and reported with their 95% confidence interval (CI). An overall treatment effect is calculated as a weighted average of the individual effect sizes (95% CI shown). Based in the four validation datasets, SMD of FSA scores between individuals with bipolar disorders and healthy controls were significantly negative (overall effect size = -6.45 , $P < 2 \times 10^{-10}$); SMD of FSA scores between individuals with bipolar disorders and schizophrenia were significantly positive (overall effect size = 3.83 , $P < .0002$). Overall the result suggests that bipolar disorder is positioned between schizophrenia and healthy controls on the FSA spectrum. Moreover, we found that FSA scores for individuals with OCD, ADHD and depression did not significantly differ from healthy comparison individuals, indicating that there is less overlap between the three neuropsychiatric disorders and schizophrenia in striatal dysfunction.



Extended Data Fig. 7 | Spatial correlation between [¹¹C] Raclopride PET imaging and fALFF t-statistic maps within the striatum and its subregions. [¹¹C] Raclopride PET image (left) and fALFF t-statistic map (right) are represented on the top. Scatter plots show the association between the t-statistic map and the marker of D2/3 receptor density within distinct striatal subregions (Pearson's r was represented below, in 1.5 mm resampled resolution): ventral caudate (orange red; left hemisphere $r=.78$, $n=1094$ voxels; right hemisphere $r=.83$, $n=764$ voxels), globus pallidus (burnt yellow; left $r=.85$ $n=758$ voxels; right $r=.72$, $n=773$ voxels), nucleus accumbens (leafy green; left $r=.51$, $n=776$ voxels; right $r=.79$, $n=958$ voxels), ventromedial putamen (lightish blue; left $r=.82$, $n=793$ voxels; right $r=.49$, $n=607$ voxels), dorsal caudate (bright lilac; left $r=.81$, $n=1178$ voxels; right $r=.84$, $n=1588$ voxels) and dorsolateral putamen (lightish red; left $r=.57$ $n=1079$ voxels; right $r=.25$, $n=1111$ voxels). The bottommost scatter plot is for the whole striatum.

